Practical Limitations to Plasma Edge Electron Temperature Measurements by Radiometry of Electron Cyclotron Emission

W. Suttrop, A.G. Peeters,
ASDEX Upgrade team, NBI group

IPP 1/306

Dezember 1996

MAX-PLANCK-INSTITUT FÜR PLASMAPHYSIK

85748 GARCHING BEI MÜNCHEN

MAX-PLANCK-INSTITUT FÜR PLASMAPHYSIK

GARCHING BEI MÜNCHEN

Practical Limitations to Plasma Edge Electron Temperature Measurements by Radiometry of Electron Cyclotron Emission

W. Suttrop, A.G. Peeters,
ASDEX Upgrade team, NBI group

IPP 1/306 Dezember 1996

Die nachstehende Arbeit wurde im Rahmen des Vertrages zwischen dem Max-Planck-Institut für Plasmaphysik und der Europäischen Atomgemeinschaft über die Zusammenarbeit auf dem Gebiete der Plasmaphysik durchgeführt.

Practical Limitations to Plasma Edge Electron Temperature Measurements by Radiometry of Electron Cyclotron Emission

W. Suttrop, A. G. Peeters,
ASDEX Upgrade team, NBI group,
Max-Planck-Institut für Plasmaphysik,
EURATOM Association, D-85748 Garching

November 14, 1996

Abstract

Various types of limitations to electron temperature measurements by radiometry of Electron Cyclotron Emission (ECE) are reviewed with respect to their practical relevance for T_e diagnostics at the edge of fusion plasmas. Low and high density limits exist due to finite optical depth and right-hand wave cut-off, respectively. The spatial resolution is limited by Doppler and relativistic broadening. A new effect is the observation of enhanced ECE at frequencies resonant at plasma edge, obtained at high T_e gradients and low density. Experimental results are presented to characterise this phenomenon and its dependence on plasma parameters. The distortion of the electron distribution function near the plasma edge necessary is estimated using Fokker-Planck simulations. It is found that the measured ECE spectra can be reproduced if enhanced diffusion of fast particles is assumed. Neo-classical transport, taking into account mirror and ripple trapped particle losses, cannot account for this transport enhancement.

Introduction

For many years by now, radiometry of Electron Cyclotron Emission (ECE) has been widely used as a diagnostics of electron temperatures in plasmas. The theoretical background to understand the applicability of the ECE diagnostics for T_e measurements and its limitations is long established (e.g., see [1]). With the availability of heterodyne receivers at frequencies relevant for ECE in fusion plasmas ($f \geq 70$ GHz) very sensitive ECE measurements with high temporal and spatial resolution have become possible. These properties would, in principle, render ECE an ideal T_e diagnostic to investigate the plasma edge, in particular in high confinement mode (H-mode), where at the same time steep gradients and fast MHD activity (Edge Localised Modes, ELMs) occur.

While in the plasma bulk, thermal black-body ECE prevails under almost all circumstances which makes interpretation of ECE measurements particularly easy, a number of limiting effects have to be taken into consideration for measurements at the plasma

edge. First the plasma will become optically thin at regions of low electron densities and temperatures, with the effect that the apparent radiation temperature T_{rad} drops below the true electron temperature T_e. However, for edge parameters of ASDEX Upgrade sufficient optical depth at the edge is obtained in almost all cases, except only for Ohmic discharges at lowest densities. Second, a pronounced enhancement of the emitted intensity above the black-body emissivity for the edge electron temperature is observed near the edge at low densities and high heating powers. This effect has by now been observed in several machines, including DIII-D [2], JET [3] and ASDEX Upgrade (this report). As yet, no satisfactory explanation for the experimental findings has been found. Several possibilities have been proposed by [4], namely shine-through of downshifted radiation from the high-energy tail of the bulk electron distribution, radiation of non-Maxwellian distributions at the plasma edge, and the special case of fast electrons generated by lower hybrid heating. The latter is discussed in more detail in [5]. In this report, we report the experimental observations of enhanced edge radiation on ASDEX Upgrade and perform a quantitative comparison with several mechanisms.

This report is organised as follows: In the first section, the various well-known limits to ECE and their influence on T_e measurements are reviewed. Examples of ECE measurements on ASDEX Upgrade are given together with handy formulas for instant interpretation of ECE results. In section 2, we discuss the phenomenon of enhanced radiation apparently originating from the plasma edge. Observations on ASDEX Upgrade are shown together with the radiation enhancement on various plasma parameters. With the classical ECE problems of section 1 in mind, several possible explanations of this effect are discussed.

1 Summary of limiting effects to ECE measurements

1.1 Principle of ECE-diagnostics

Radiometry of the electron cyclotron emission (ECE) is used by now on many fusion devices as a diagnostics of radial profiles of the electron temperature T_e. This well-established method is based on the spectral measurement of the absolute millimetre wave intensity $I(f)$.

The measurement frequency f is determined by the cyclotron resonance

$$f = \omega/2\pi = l \times e\, B/(2\pi m_e), \tag{1}$$

with l being the harmonic number (2 in most cases), B the total magnetic field, e the elementary charge and m_e the electron mass in the laboratory frame. In a toroidal device, $B = B(r)$, leading to radial resolution of ECE measurements even with a single sightline. On ASDEX Upgrade, the toroidal field $B_t = B_0 \times R_0/R$ can vary between ≈ 1 T to 4.9 T (at various radial locations) leading to a large frequency span of $f = 55 \ldots 270$ GHz to be covered in the second harmonic.

For a black-body source, I depends solely on the source temperature T. The source of electron cyclotron emission is radiation from the the electron gyromotion, hence, for a Maxwellian velocity distribution perpendicular to the magnetic field, $T = T_{e,\perp}$ (We abbreviate $T_{e,\perp}$ by T_e in the following).

The black-body intensity I_{BB}, radiated power per unit area and unit solid angle, is given by Planck's law

$$I_{BB}\mathrm{d}\omega = \frac{\hbar\omega^3}{8\pi^3c^3}\ \frac{1}{(\exp(\hbar\omega/kT_e-1))}\mathrm{d}\omega = \frac{hf^3}{c^3}\ \frac{1}{(\exp(hf/kT_e-1))}\mathrm{d}f,$$

where $\mathrm{d}f$ and $\mathrm{d}\omega$ denote the observed frequency interval and angular frequency interval, respectively. For present day fusion plasmas ($h\nu < 1$ meV, $kT > 10$ eV), $h\nu << kT$ and hence the Rayleigh-Jeans approximation holds

$$I_{BB} = \frac{\omega^2}{8\pi^3c^3}kT_e. \tag{2}$$

As a standard, the evaluation of electron temperature profiles is based on equations 1 and 2, assuming that the relativistic frequency shift is small compared to the frequency resolution of the instrument (and hence can be neglected) and that the electron cyclotron emission is optically thick (the plasma is a black body at the particular measurement frequency). We will examine both assumptions in the next sections. The examples are taken from ECE measurements with the 48-channel heterodyne radiometer installed at the ASDEX Upgrade tokamak.

1.2 High density limit: cut-off

An upper limit to the electron density is given by the accessibility of the resonant location from the outside of the plasma. Extraordinary mode waves (with frequency $f = \omega/2\pi$) become evanescent when, on the ray path, $\omega < \omega_R$, where $\omega_R = (\omega_c + \sqrt{\omega_c^2 + 4\omega_p^2})/2$ is the right-hand cut-off frequency, or, eliminating ω_R, $\omega_p^2 > \omega^2 - \omega\omega_c$.

For the l-th harmonic ($l \geq 2$) of the cyclotron frequency $\omega = l\omega_c$, X-mode right-hand cut-off occurs when $\omega_p^2 > l(l-1)\omega_c^2$, corresponding to the critical electron density

$$n_{crit}^{X,l} = \frac{l-1}{l}\frac{\epsilon_0 m_e}{q^2}\omega^2 = 1.24\times10^{16}\mathrm{m}^{-3}\mathrm{GHz}^{-2}\times\frac{l-1}{l}f^2,$$

or, in terms of the local magnetic field B,

$$n_{crit}^{X,l} = l(l-1)\frac{\epsilon_0}{m_e}B^2.$$

Usually, the second harmonic ($l = 2$) is observed, so that

$$n_{crit}^{X2} = 1.94\times10^{19}\mathrm{m}^{-3}\mathrm{T}^{-2}\times B^2.$$

In ordinary mode, cut-off occurs below the plasma frequency ($\omega \leq \omega_p$), or above

$$n_{crit}^{O,l} = l^2\frac{\epsilon_0}{m_e}B^2.$$

The effect of right hand cut-off on ECE radiation temperature profiles is illustrated in Fig. 1. Radial profiles of the second harmonic cyclotron frequency ($2f_r$) and the evanescent interval between the upper hybrid frequency f_{uh} and the right-hand cut-off frequency f_r can immediately be used to determine the regions of right-hand cut-off. In Fig. 1 a) a

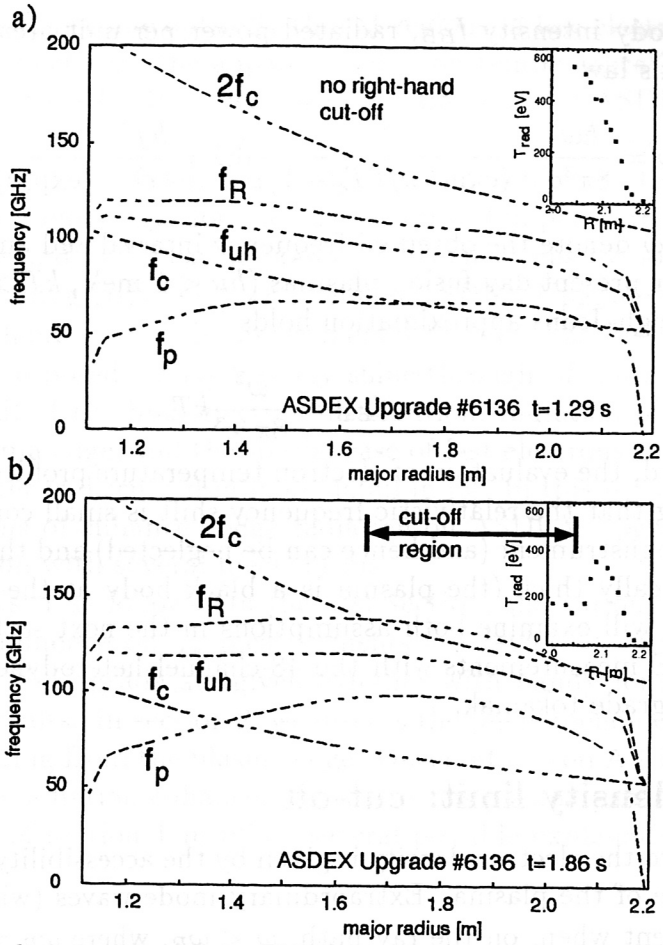

Figure 1: *First (f_c) and second harmonic ($2f_c$) of the cyclotron frequency, plasma- (f_p), upper hybrid (f_{uh}), and right-hand cut-off frequency (f_R) vs. major radius for 2 cases: (a) no right-hand cut-off (b) right-hand cut-off. The cut-off condition in X2-mode is reached whenever f_r rises above the measurement frequency $2f$. In this case, the observed intensity strongly decreases (as shown by the ECE profiles in the inserts)*

phase of ASDEX Upgrade H-mode discharge #6136 not in cut-off is shown. Consequently, the edge electron temperature profile is unperturbed, showing a steep monotonous rise of T_e inside the separatrix. Note from the relations above that the critical cut-off density in first harmonic O-mode is half of that for second harmonic X-mode. Over most of the low-field side in the case of Fig. 1 a), the electron density high enough for first harmonic O-mode cut-off, but too low for second harmonic X-mode cut-off. Hence it is very desirable to use high harmonics for ECE diagnostics, but the necessary optical thickness and harmonic overlap in low aspect-ratio machines (see paragraphs below) impose a practical restriction to the second harmonic X-mode in most cases.

With further increased density, at a later time during the same discharge, X-mode cut-off is reached. This is seen in Fig. 1 b) by the evanescent frequency interval between f_{uh} and f_R now overlapping the second harmonic cyclotron resonance within a significant radial range (between 1.65 m and 2.05 m major radius). Consequently, T_{rad} in this interval drops to low value and is not representative for T_e any more. However, the ECE signal does not completely vanish, because some radiation from above and below midplane (at larger effective plasma radii) can reach the ECE antenna by multiple reflection at the

cut-off layer and at the vessel wall on the low-field side, or, for propagation not parallel to density gradients, by refraction.

In summary, the cut-off condition is very well understood and clearly predictable. Routine checks are easily possible but call for a density diagnostics accurate enough to evaluate $f_R(R,t)$ with sufficient radial and temporal resolution (such as to match the ECE measurement).

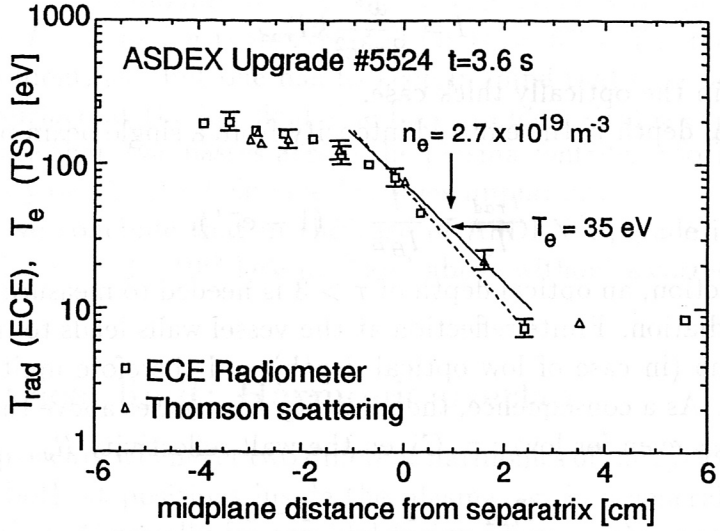

Figure 2: *Comparison of a T_e profile from Thomson scattering and T_{rad} from ECE at the edge of an Ohmic discharge. Low optical depth outside the separatrix causes a discrepancy for $n_e T_e \leq 1 \times 10^{18}$ keV m^{-3}*

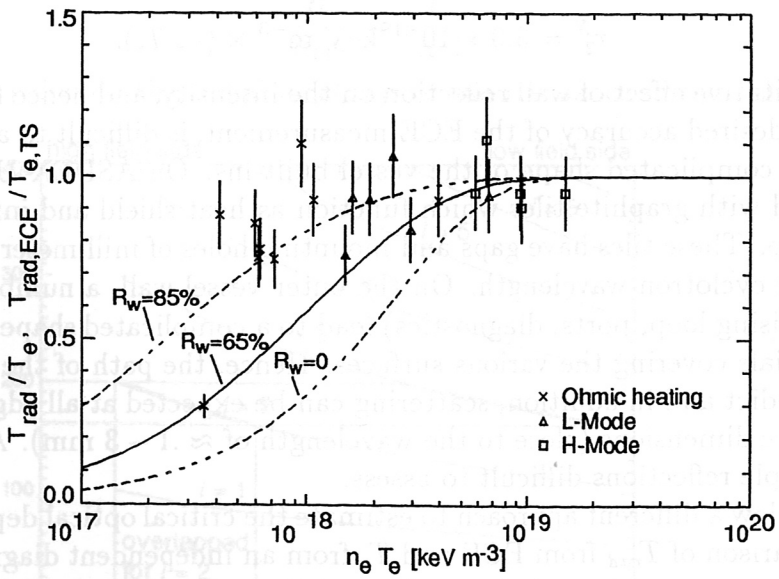

Figure 3: *Ratio $T_{rad,ECE}/T_e$ (T_e from Thomson scattering) as a function of the optical depth parameter $n_e T_e$. The lines are calculated from Eq. 3 for various values of the wall reflectivity R.*

1.3 Low density limit: finite optical depth

As mentioned in section 1.1, the measured ECE intensity equals the black-body intensity (Eq. 2) only in the case of high optical depth $\tau = \int \alpha(r)dr$, or high absorption α over sufficient ray path length r, i.e. when the plasma is opaque at the measurement frequency. At high optical depth, the measured intensity is then proportional to T_e and does not depend on n_e. Conveniently, the measured intensity I is expressed in terms of the radiation temperature T_{rad},

$$I = \frac{\omega^2}{8\pi^3 c^2} k T_{rad},$$

so that $T_{rad} = T_e$ in the optically thick case.

At finite optical depth τ, the emitted intensity from a single beam pass through a slab of plasma is

$$\frac{T_{rad}}{T_e} = \frac{I}{I_{BB}} = (1 - \mathrm{e}^{-\tau}).$$

Without wall reflection, an optical depth of $\tau > 3$ is needed to measure more than 95% of the black-body radiation. Finite reflection at the vessel walls leads to multiple ray passes through the plasma (in case of low optical depth) and therefore multiple absorption at the resonant layer. As a consequence, the intensity I increases above the single pass value and approaches I_{BB} even for lower τ. Given the wall reflectivity R_w,

$$\frac{T_{rad}}{T_e} = \frac{I}{I_{BB}} = \frac{1 - e^{-\tau}}{1 - R_w \mathrm{e}^{-\tau}}. \tag{3}$$

The optical depth τ of cyclotron absorption in an inhomogeneous B-field is given by, e.g., [1]. For $l = 2$ and $< A_l >= 1$, and typical ASDEX Upgrade parameters at the plasma edge at the low field side ($L_B = R = 2.15$ m, $B(R) = 2$ T),

$$\tau_2^X = 3.9 \times 10^{-19} \mathrm{keV\ m^{-3}} \times (n_e\, T_e).$$

The quantitative effect of wall reflection on the intensity, and hence the critical optical depth τ for a desired accuracy of the ECE measurement, is difficult to assess. Among the reasons is the complicated shape of the vessel built-ins. On ASDEX Upgrade, the inner wall is covered with graphite tiles which function as heat shield and inner limiter during plasma startup. These tiles have gaps and mounting holes of millimeter dimensions, comparable to the cyclotron wavelength. On the outer vessel wall, a number of installations (passive stabilising loop, ports, diagnostics) lead to a complicated shape with a number of various materials covering the various surfaces. Hence, the path of the reflected beam is difficult to predict and in addition, scattering can be expected at all edges and structures with millimetre dimensions (close to the wavelength of $\approx .1 - 3$ mm). All this makes the effect of multiple reflections difficult to assess.

Here we follow a different approach to estimate the critical optical depth τ by an experimental comparison of T_{rad} from ECE and T_e from an independent diagnostics (Thomson scattering, in our case). Figure 2 shows T_{rad} and T_e profiles during an ohmic phase of ASDEX Upgrade discharge #5524. Within error bars, both measurements agree inside the separatrix ($r < a$). A significant discrepancy is found below $T_e = 35$ eV and $n_e = 2.7 \times 10^{19}$ $\mathrm{m^{-3}}$ (corresponding to $\tau \approx 0.3$).

We will now check the dependence of the ratio $T_{rad}(\mathrm{ECE})/T_e(\mathrm{Thomson})$ as a function of $T_e \times n_e$ (all quantities taken at the nominal separatrix position) during Ohmic, L-mode

and H-mode density scans (data points in Fig. 3). In discharges down to $T_e \times n_e = 4 \times 10^{17}$ keV m^{-3}, T_{rad} is found to be less than 30 % below T_e. For comparison, the ratio expected from Eq. 3 is plotted for various values of the wall reflectivity coefficient $R_w = 0$ (single pass absorption), $R_w = 65\%$ (reflectivity of plane graphite surface), and $R_w = 85\%$. In a laboratory test, the reflectivity of graphite surfaces machined similar to the graphite tiles of the inner heat shield was found to be 65% at near normal incidence. Hence, the curve for $R_w = 65\%$ is expected to describe the situation best. Accordingly, at $T_e \times n_e = 3 \times 10^{18}$ keV m^{-3} ($\tau = 1$), T_{rad} amounts to 85% of T_e, consistent with the experimental data. Below that point, T_{rad} is higher than expected for $R_w = 65\%$. The reason for this feature has not yet been identified, but one has to keep in mind that on a large fraction area of the inner vessel surface at the low field side bare stainless steel is exposed. For very low optical depth, more than two passes across the plasma contribute to T_{rad} and in this case the wall reflectivity on the low field side becomes important.

In summary, we conclude that in the case of ASDEX Upgrade it is safe to identify T_{rad} with T_e at $T_e \times n_e = 3 \times 10^{18}$ keV m^{-3} and above without a correction for low optical depth.

1.4 Geometrical limit: Harmonic overlap

Harmonic overlap occurs whenever two different harmonics of the cyclotron frequency have their resonances both at positions inside the plasma, or, in a general sense, at locations of non-zero emission. Generally for toroidal fusion plasmas, the contribution of internal plasma currents to the total magnetic field is small (in a tokamak, $B_p^2 \ll B_t^2$), so that in practice harmonic overlapped regions are defined geometrically regardless of plasma parameters. Taking $B(R) = B_0 R_0 / R$, emission from the l-th harmonic overlaps with the $(l \pm 1)$-th harmonic for

$$\frac{R_l}{R_{l\pm1}} = \frac{l}{l \pm 1},$$

where R_l and $R_{\pm1}$ denote the radial locations of the resonance in the l-th and $(l \pm 1)$-th harmonic.

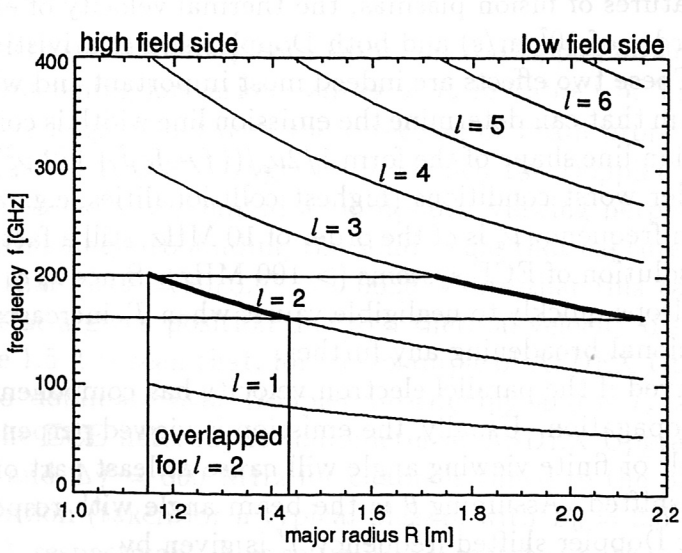

Figure 4: *Harmonic overlap of the second and third harmonic on ASDEX Upgrade.*

Figure 4 is a sketch of harmonic overlap on ASDEX Upgrade, showing the overlap of the second harmonic at $R \leq 1.43$ with the third harmonic at $R \leq 2.15$ m. When

viewing from the low field side, second harmonic emission from a location on the high-field side at ($R < 1.43$) has to cross a region with third harmonic resonance inside the plasma where absorption and (grey) emission can occur. Depending on the optical depth of the third harmonic, either the second or the third harmonic or a superposition of both will be observed. Measurements at the high-field side are therefore preferably conducted by viewing from the high field side, because the second harmonic can then be detected without crossing the overlapped third harmonic region. In case high optical depth of the second harmonic, the third harmonic emission will in principle be absorbed at the second harmonic resonance. Thus, an unperturbed measurement in the overlapped region is possible under ideal conditions.

Harmonic l	at radius R_l (m)	overlaps with $l+1$	at radius R_{l+1} (m)
2	$1.15 - 1.43$	3	$1.725 - 2.15$
3	$1.15 - 1.61$	4	$1.53 - 2.15$
4	$1.15 - 1.72$	5	$1.44 - 2.15$

Table 1: Harmonically overlapped radii on ASDEX Upgrade for various harmonics of the electron cyclotron frequency.

For ASDEX Upgrade (aspect ratio 3.3), most plasmas extend from an inner boundary at $R = 1.15$ m (at midplane) to an outer boundary at $R = 2.15$ m. The corresponding harmonically overlapped regions for the various harmonics are listed in Table 1.4. Edge measurements are harmonically overlapped at the high field side in the second harmonic and on both sides in the third harmonic. The fourth and higher harmonics are completely overlapped.

1.5 Resolution limit: Relativistic and Doppler frequency shifts

Because of high temperatures of fusion plasmas, the thermal velocity of electrons is considerable (v_{th} is of the order of 10^7 m/s) and both Doppler and relativistic shifts have to be taken into account. These two effects are indeed most important and will be discussed below. A third mechanism that can determine the emission line width is collision broadening, leading to a Lorentzian line shape of the form $1/2\nu_c/((f-f_0)^2+1/2\,\nu_c^2)$. However, for fusion plasmas even under worst conditions (highest collisionalities, e.g. $n_e = 10^{20}$ m^{-3}, $T_e = 10$ eV), the collision frequency ν_c is of the order of 10 MHz, still a factor of ten below the typical frequency resolution of ECE systems (> 100 MHz). Since $\nu_c \propto T^{-3/2}$, the collisional resolution limit drops quickly to negligible values when T_e increases. Accordingly, we do not consider collisional broadening any further.

Doppler shift is observed if the parallel electron velocity has components in the direction of the ECE wave propagation. Usually, the emission is viewed perpendicular to field lines, but any antenna tilt or finite viewing angle will cause at least part of the measured intensity to be Doppler shifted. Assuming θ is the beam angle with respect to the field direction, the relativistic Doppler shifted frequency f' is given by

$$f'_{\text{Doppler}} = f\sqrt{\frac{1-\frac{v}{c}\cos\theta}{1+\frac{v}{c}\cos\theta}} \approx f(1-\frac{v}{c}\cos\theta). \qquad (4)$$

The sign of v determines whether f is up- or down-shifted. Since usually the drift velocity $v_D = j/(ne) \approx 10^5$ m/s is much smaller than the electron thermal velocity, Doppler shift results in spectral broadening, but negligible frequency shift of the emission maximum. For a thermal distribution, the relevant velocity component is the mean thermal velocity parallel to $\vec{B}$, or $v_{||} = \sqrt{kT/m_e}$.

Relativistic time dilatation (or equivalently, mass increase) leads to a down-shift of the frequency (in the laboratory rest frame)

$$f'_{\text{Relativistic}} = f \frac{1}{\sqrt{1 - v^2/c^2}}.$$

All three velocity components contribute to the relativistic shift. In order to avoid calculating the relativistic velocity, we consider the electron mass increase (in the laboratory frame) as a function of kinetic energy. From $E_{\text{kin}} = m_c^2 - m_0c^2 = (m - m_0)c^2 = \Delta mc^2$ we obtain the relative frequency shift $\Delta f/f = \Delta m/m = E_{\text{kin}}/m_0c^2$. One can estimate the relative frequency shift of the emission maximum from the maximum of the Maxwellian velocity distribution (at $E_{\text{kin}} = kT/2$) and obtain the line width to be the relative frequency shift at FWHM of the distribution ($0.05kT < E_{\text{kin}} < 1.85kT$ or $\Delta E = 1.8kT$).

T_e (keV)	$(\sqrt{kT/m})\ /\ c$ (v/c)	$\Delta f/f$, Doppler broadening	$\Delta f/f$, Relativistic shift	broadening
0.01	0.0044	0.0003	10^{-5}	2×10^{-5}
0.1	0.014	0.0009	10^{-4}	2×10^{-4}
1	0.044	0.003	0.001	0.002
10	0.14	0.009	0.01	0.02

Table 2: Relative frequency shifts due to Doppler broadening and relativistic shift and broadening for various values of T_e. Doppler shift is calculated for $\cos\theta = 0.0628$ (ASDEX Upgrade case)

We quantify the relative frequency shifts due to Doppler broadening as well as relativistic shift and broadening for various values of T_e in Table 1.5. The only device-dependent parameter is the angle θ between the direction of beam propagation and the magnetic field. In the case of ASDEX Upgrade, for which the Doppler shift is calculated in Table 1.5, the antennae are mounted at midplane, viewing perpendicular to the magnetic field. The viewing angle (bounding the solid angle that captures 90 % of the RF power) is $2 \times 3.6°$ so that $\cos\theta = \sin 3.6° = 0.0628$. Note that this calculation only yields the frequency shift at a given position due to a thermal velocity distribution.

From Table 1.5 it is seen that, for the example of ASDEX Upgrade, relativistic broadening starts to dominate over Doppler broadening above $T_e \approx 1$ keV. The frequency resolution of the ECE heterodyne radiometer at ASDEX Upgrade is $\Delta f = 300$ MHz for edge channels and $\Delta f = 600$ MHz for channels tuned to the plasma centre. The corresponding resolution (taken for a typical plasma with $B_0 = 2.5$ T) is $\Delta f/f = 0.003$ and $\Delta f/f = 0.0043$, respectively. This setup is well matched to the resolution limit for $kT \approx 1$ keV (plasma edge) and $kT \approx 2$ keV (plasma centre). Below 1 keV, the frequency resolution and therefore the radial resolution is determined by the bandwidth of the receiver, rather than by line broadening.

The corresponding radial resolution is obtained from the frequency resolution simply by

$$\Delta R = \frac{\partial R}{\partial f}\Delta f = \frac{l}{2\pi}\frac{eB_0R_0}{m_e f^2}\Delta f = R\frac{\Delta f}{f}.$$

For $T_e = 100$ eV ($\Delta f/f \approx 0.001$), the maximum radial resolution possible at $R = 2.15$ m (plasma edge at the low field side on ASDEX Upgrade) is 2 mm. At 1 keV, the resolution limit is at about 8 mm. Extrapolating to the centre of a burning fusion plasma, (say, ITER assuming $R = 8.1$ m, $kT_e \approx 30$ keV), the radial resolution can deteriorate significantly up to $\Delta R \approx 30$ cm. This and other implications for an ECE diagnostics on ITER are discussed in more detail in Ref. [6].

Note that the above estimate of the resolution limit takes into account only the variation of $B(R)$. In the optically thick case, radiation emitted inside a slab of width ΔR can be re-absorbed and only a thin layer near the resonance location contributes to the radiation visible from outside. The width of this layer is determined by the distance between onset of absorption and the location R at which the integrated absorption coefficient or "local optical depth" becomes sufficient for nearly complete absorption

$$\tau(R) = \int_R^\infty \alpha(r)\mathrm{d}r \approx 3.$$

1.6 Sensitivity limit: Plasma noise

A fundamental limit to the minimum changes of T_e that can be resolved by ECE measurements is set by the noise in black-body radiation emitted from the plasma. This limit exists for all black-body sources and comes in independent of the noise produced by the RF receiver (actually, the instrumental noise of state-of-the-art heterodyne ECE receivers is much smaller than the noise emitted by a fusion plasma). The radiated intensity fluctuates even when the electron temperature is constant. This fluctuation appears as white noise in the measurement with an r.m.s. value given by the so-called radiometer formula

$$\Delta T_{rad} = T_{rad} \times \sqrt{\frac{\Delta f_v}{\Delta f_{RF}}}, \tag{5}$$

where Δf_{RF} is the receiver radio frequency bandwidth and Δf_v is the video bandwidth, i.e. the bandwidth of the system after RF power detection. For a derivation of the radiometer formula, e.g. see [7].

Eq. 5 has two immediately intuitive aspects. First, the total RF power collected by the antenna is proportional to the RF bandwidth Δf_{RF} of the system. Since black-body fluctuations at different radiation frequencies are uncorrelated, the noise power is proportional to $\sqrt{\Delta f_{RF}}$ and the signal-to-noise ratio (SNR) increases with RF bandwidth. Because in the Rayleigh-Jeans limit the RF power directly corresponds to temperature, ($T/\Delta T = P/\Delta P \propto \sqrt{\Delta f_{RF}}$). Second, the amplitude signal obtained by detection of the RF power also has a white noise spectrum (this is not immediately obvious but explained in Ref. [7]). This means that the noise, uncorrelated at different video frequencies, will increase with the square root of the video bandwidth $\sqrt{\Delta f_v}$. As long as the video bandwidth is high enough not to truncate the signal spectrum, the signal amplitude is independent of Δf_v. As a result, the SNR is proportional to $1/\sqrt{\Delta f_v}$.

An unfortunate property of radiometry is, therefore, that a good temperature resolution can be achieved only at the expense of either long integration time (low video

bandwidth) or low radial resolution (high RF bandwidth). For fusion applications, the video bandwidth is dictated by the time scale of plasma activities of interest and the RF bandwidth is determined by the desired radial resolution, and in most cases set close to the resolution limit (see section 1.5).

As example, consider the case of ASDEX Upgrade where one might want to resolve MHD activity with $\Delta f_v = 300$ kHz bandwidth at the plasma edge using an RF bandwidth $\Delta f_{RF} = 300$ MHz for ≈ 6 mm radial resolution. The r.m.s. noise level obtained would be $\Delta T/T = 1/\sqrt{1000} \approx 3\%$. For $T_e = 100$ eV, this translates into peak-to-peak noise of $\Delta T_{p-p} = \sqrt{2} \times 2 \times T/\sqrt{1000} \approx 9$ eV or almost 10% of the signal! It is therefore wise to carefully select the RF and video bandwidths according to the experiment to be undertaken. The most flexible, but costly approach is to record a large number of channels with narrow RF frequency intervals (close to the resolution limit) at high video bandwidth, so that filters in the space and time domain can be applied *ex post* to cut-out the noise fraction which is spectrally separated from the signal. An example is the detection of modulated plasma heating (e.g. by ECRH) over a time interval Δt of the order of 1 s duration. After Fourier transform of the T_e traces, the fixed modulation frequency ideally appears in only one frequency bin thus limiting the video bandwidth to $\Delta f_v = 1/\Delta t \approx 1$ Hz. In principle, detection of the amplitude and phase of the T_e response to the modulation can be achieved with a very good SNR of $T/\Delta T = \sqrt{300 \text{ MHz}/1 \text{ Hz}} \approx 5 \times 10^5$. In practice, a modulation of less than $\Delta T = 0.1$ eV on a background of $T = 1000$ eV can be well resolved.

Bandwidth selection will fail if the signal of interest has a large inherent bandwidth, such as electron temperature fluctuations. Generally, T_e fluctuations are much smaller than the plasma noise under which they are buried regardless of the video bandwidth of the system. Several techniques have been demonstrated to overcome this problem by correlation techniques, in particular correlation of independent measurements at the same frequency but different viewing angles for which the plasma noise is decorrelated [8] and measurement of separate but closely spaced frequency intervals collecting emission from different portions of the energy distribution function at the same position [7, 9].

2 Enhanced ECE radiation from the plasma edge

In the remainder of this report, we discuss the phenomenon of enhanced ECE radiation apparently originating from the plasma edge. This effect has been observed on several machines ([2, 3] and ASDEX Upgrade, this report), but no conclusive and quantitative explanation has been given to date. In the following paragraphs, we first present experimental data taken from ECE measurements on ASDEX Upgrade and then examine a number of possible explanations for the observed phenomenon.

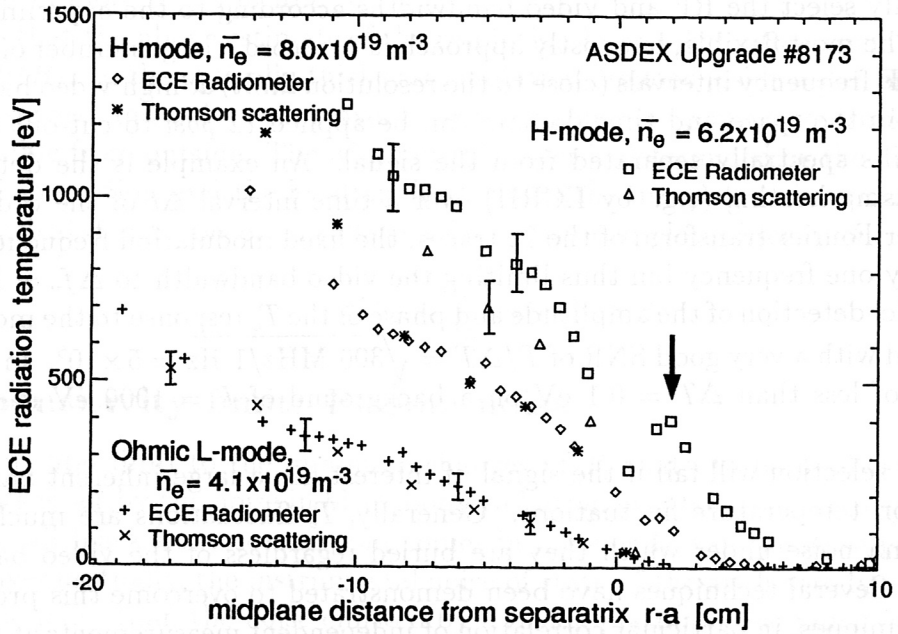

Figure 5: *Edge T_{rad} profiles from ECE during different phases of one ASDEX Upgrade discharge. During H-mode, T_{rad} rises above T_e (derived from Thomson scattering) with a local maximum appearing close to the separatrix (marked by the arrow).*

2.1 Experimental observations of enhanced ECE radiation

It is an experimental observation that, under certain circumstances, the ECE emission at frequencies resonant close to the plasma edge rises above the level of black-body radiation corresponding to electron temperatures at this position. The appearance of this phenomenon is demonstrated in Fig. 5 for various time slices of the same discharge, ASDEX Upgrade shot #8173 (I_p = 1 MA, B_0 = 2.5 T, ion-grad B drift towards X-point). For three phases of the discharge, the electron temperature obtained from Thomson scattering is compared with the radiation temperature from ECE. The ECE data is plotted against the resonance location for each channel frequency. While during the Ohmic phase ("Ohmic L-mode") and H-mode at higher electron density $\bar{n}_e = 8 \times 10^{19}$ m^{-3} both diagnostics are in reasonable agreement at the plasma edge, there is a significant discrepancy during H-mode at lower density $\bar{n}_e = 6.2 \times 10^{19}$ m^{-3}. The ECE radiation temperature rises above T_e (as derived from Thomson scattering) inside the separatrix (about 15% at $r = a - 5$ cm). In addition, a pronounced feature of enhanced T_{rad} (radiation "hump",

marked by an arrow in the figure) appears at frequencies resonant outside the separatrix (with maximum at $r = a + 2$ cm).

This enhancement of cyclotron radiation cannot simply be subsumized under one of the effects discussed in section 1. Neither high density cut-off nor low optical depth can result in an enhancement of radiation temperature above T_e. Also, the affected radial range at the plasma edge on the low field side is not harmonically overlapped in the second harmonic.

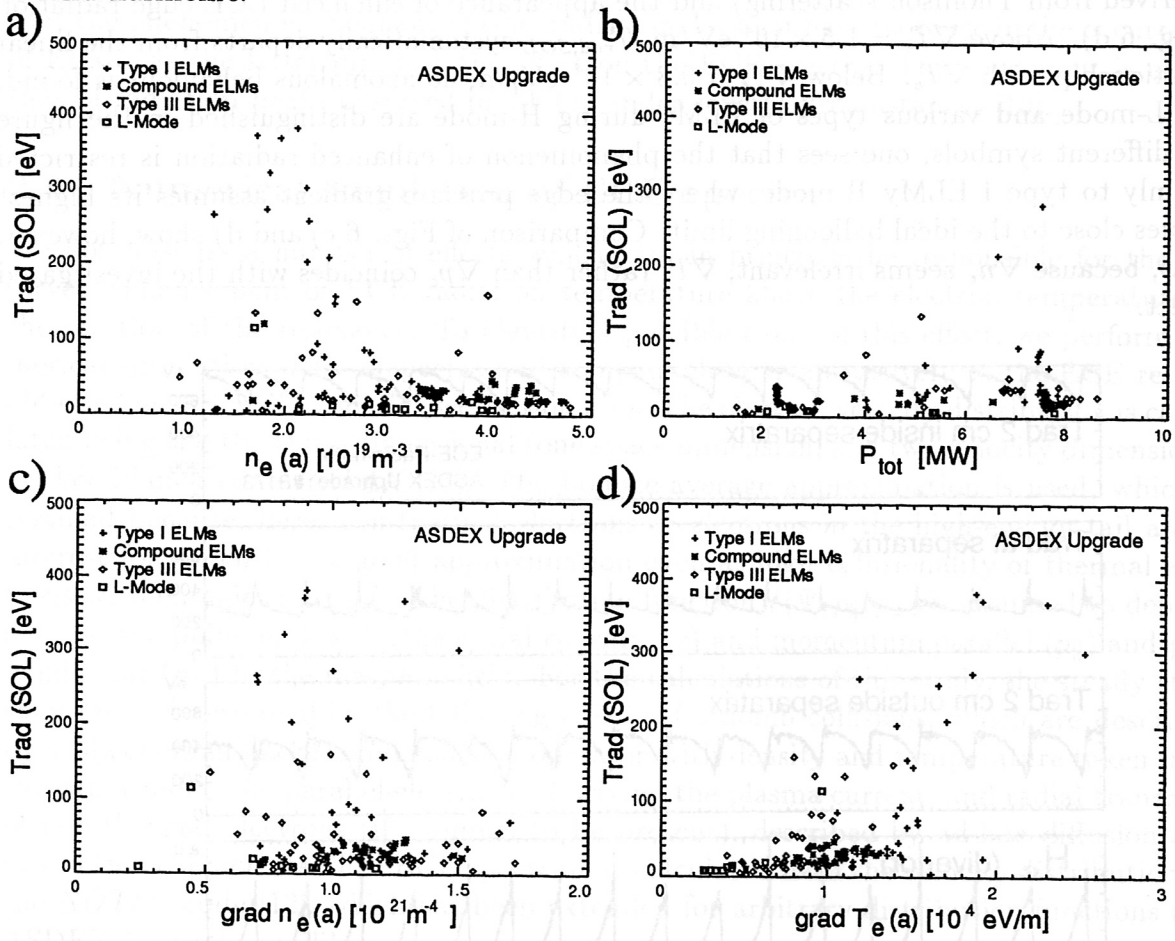

Figure 6: *Apparent ECE radiation temperature at a frequency resonant in the SOL (2 cm outside separatrix) as a function of various plasma parameters: a) electron density at the separatrix, b) total heating power, c) electron density gradient, and d) electron temperature gradient*

We now identify the conditions under which enhanced ECE radiation appears. To this end, we plot the apparent radiation temperature at $r = a + 2$ cm (denoted by $T_{rad,SOL}$) as a function of various plasma parameters (Fig. 6) We randomly select a range of several dozen deuterium discharges on ASDEX Upgrade performed during 1996 with a variety of magnetic fields, plasma currents, densities, auxiliary heating powers, etc. This set contains L-modes and H-modes at low and at high radiation levels with various types of Edge Localised Modes (ELMs). The temperature fall-off length is approximately $\lambda_T = 1.5$ cm in all regimes with very little variation, so the thermal contribution to $T_{rad,SOL}$ is a factor of $\exp(2/1.5) \approx 4$ below $T_e(a)$. For the discharges investigated, T_e at $r = a + 2$ cm is below 50 eV. Consequently, any ECE reading above this value can be taken as a measure of enhanced radiation.

When plotting $T_{rad,SOL}$ against the electron density at the separatrix (as measured by the Li-beam diagnostics), one finds that low edge density is a necessary, but not sufficient condition for enhanced radiation (Fig. 6 a). Also, enhanced radiation tends to appear at high heating power (Fig. 6 b). Note that all phases with heating powers above 2 MW are neutral-beam heated. No dependence on the density gradient is found (Fig. 6 c). The most unambiguous relation exists between the edge electron temperature gradient (derived from Thomson scattering) and the appearance of enhanced ECE edge radiation (Fig. 6 d). Above $\nabla T_e = 1.5 \times 10^4$ eV/m, $T_{rad,SOL}$ systematically departs from the linear relationship with ∇T_e. Below $\nabla T_e = 0.8 \times 10^4$ eV/m, no anomalous behaviour is found. As L-mode and various types of ELMs during H-mode are distinguished in the figure by different symbols, one sees that the phenomenon of enhanced radiation is restricted mainly to type I ELMy H-mode, where the edge pressure gradient assumes its highest values close to the ideal ballooning limit. Comparison of Figs. 6 c) and d) show, however, that, because ∇n_e seems irrelevant, ∇T_e rather than ∇p_e coincides with the investigated effect.

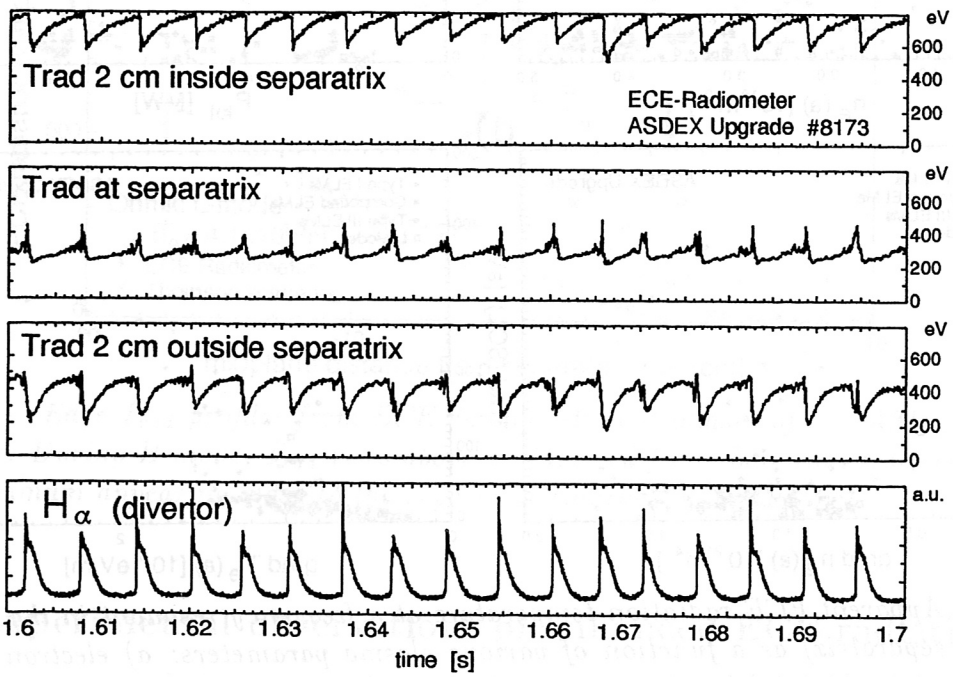

Figure 7: *Traces of T_{rad} measured at frequencies resonant 2 cm inside the separatrix ($a - 2$ cm), at the separatrix, and 2 cm outside the separatrix ($a + 2$ cm). Edge localised modes (ELMs) are detected as spikes in the divertor H_α signal. The enhanced signal apparent at $a + 2$ cm grows in between ELMs and drops during ELMs.*

We have seen that enhanced ECE radiation appears predominantly during H-modes with type I ELMs, so we may question the relationship of ELMs to the observed phenomenon. Fig. 7 shows time traces of three ECE radiometer edge channels during a phase of ASDEX Upgrade discharge #8173 with pronounced enhanced radiation (taken around the time of the topmost profile of Fig. 5). The ELMs are detected as spikes in the H_α light from the divertor, indicating enhanced particle and energy transport across the separatrix during short time intervals (< 2 ms). Accordingly, T_e inside the separatrix, as indicated by the top T_{rad} trace, drops during each ELM. At the separatrix, T_{rad} is inverted, i.e. increases during ELMs due to a brief flattening of the T_e profile during the

phase of enhanced transport. This property of ELMs is well known and observed also by other diagnostics, independent of the phenomenon of enhanced ECE radiation. The new feature arising with enhanced radiation is that the high radiation temperature detected at frequencies resonant outside the separatrix shows the non-inverted time dependence. This behaviour is in contrast with the channel tuned to the separatrix, but similar to T_e *inside* the separatrix (or, to be more precise, inside the ELM inversion radius), i.e. $T_{rad,SOL}$ drops during ELMs and recovers to high values in between ELMs. We conclude that the phenomenon of enhanced edge radiation does not have its cause in the occurrence of ELMs, as the latter diminish the effect on the ECE spectra. This behaviour is unlike that of radiation peaks observed in TFTR under several circumstances [10].

2.2 Numerical simulation of ECE spectra

We now discuss a number of effects which can, in principle, be responsible for the observed enhancement of ECE radiation temperature above the electron temperature at the position of the resonance. To identify a possible cause of this effect, we perform numerical simulation of ECE spectra and compare these quantitatively to the ECE results obtained on ASDEX Upgrade (see section 2.1). The electron velocity distribution is calculated using the the three-dimensional (one space dimension, and two velocity dimensions) Fokker-Planck code *RELAX* [11]. The bounce-average approximation is used, which is justified because, here, non-thermal electrons or electrons in the high-energy tail are of interest for which it is a good approximation even at high collisionality of thermal electrons with energies near kT. The distribution function $f(\Psi, p_\parallel, p_\perp)$ is assumed to depend only on the poloidal flux Ψ (the radial coordinate) and momentum parallel ($p_\parallel$) and perpendicular ($p_\perp$) to the magnetic field. For the calculations of this study, the steady state solution is determined by the following effects: Coulomb collisions, which are described by a Maxwellian background collision operator with density and temperature taken from the experiment, the parallel electric field driving the plasma current, and radial transport of non-thermal electrons (if assumed to be present), described by ad-hoc diffusion and convection coefficients. The ECE spectrum is calculated from the velocity distribution by the *NOTEC* code [12], which has been extended for arbitrary distribution functions and ASDEX Upgrade equilibria.

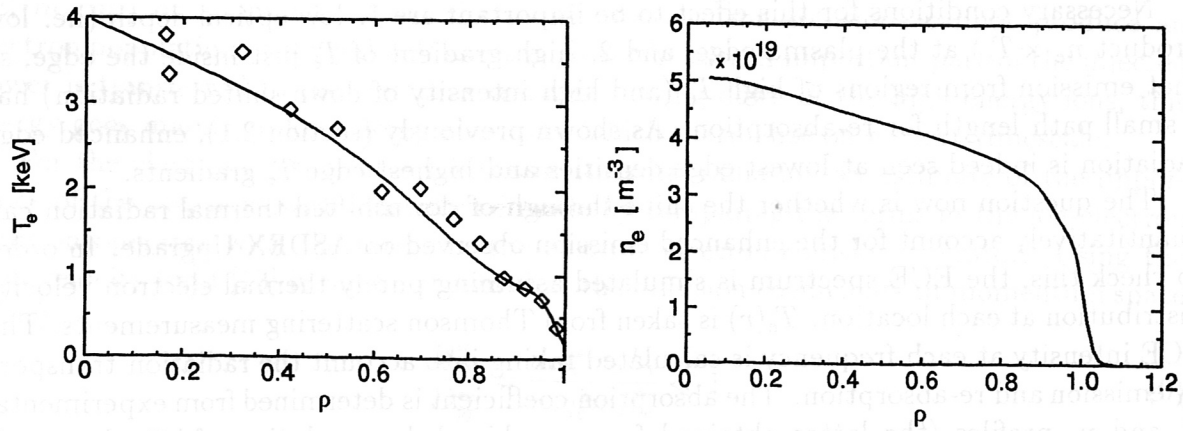

Figure 8: *Experimental T_e (Thomson scattering, symbols) and n_e profiles (DCN interferometer + Li-beam) used for the simulation of the radiation temperatures.*

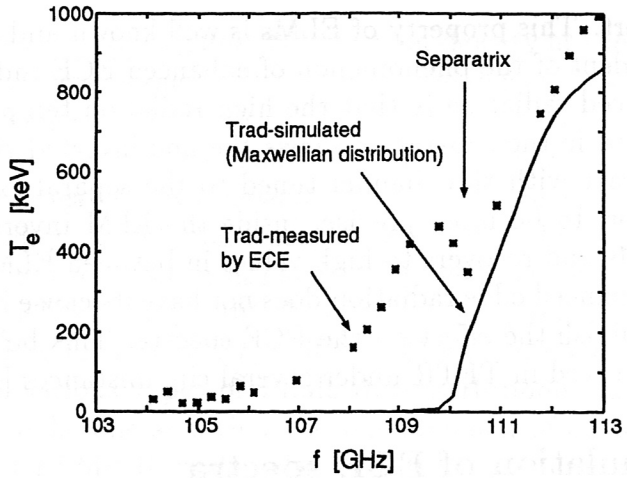

Figure 9: *Simulated T_{rad} spectrum (solid line) compared to T_{rad} spectrum measured by ECE (symbols). A thermal plasma, i.e. purely Maxwellian velocity distribution at each radial location is assumed for the simulation. Relativistic downshift and optical depth are calculated using experimental T_e and n_e profiles from Thomson scattering and Li-beam measurements.*

2.3 Radiation from a thermal plasma with low optical depth

First, we consider ECE spectra of strictly Maxwellian velocity distributions at each spatial location, but low optical depth at the edge, i.e. close to the region of large temperature gradients in H-mode. For the case of JET plasmas, it has been shown by Airoldi and Ramponi [4] that a local emission maximum at frequencies resonant to the optically thin region at the edge can occur under these conditions. When viewing the plasma from the low field side, down-shifted radiation from medium to high energy electrons of the thermal distribution inside the separatrix will normally (in optically thick conditions) be absorbed by the bulk of thermal electrons at the plasma edge. If the plasma edge is optically thin, this radiation may shine through and possibly result in a radiation temperature which can be higher than the true edge electron temperature at the resonance position. (Note that on the high field side, the edge layer has higher resonance frequencies than the hot plasma inside and cannot absorb down-shifted radiation at all, regardless of the optical depth.)

Necessary conditions for this effect to be important are 1. low optical depth (i.e. low product $n_e \times T_e$) at the plasma edge, and 2. high gradient of T_e just inside the edge, so that emission from regions of high T_e (and high intensity of down-shifted radiation) has a small path length for re-absorption. As shown previously (section 2.1), enhanced edge radiation is indeed seen at lowest edge densities and highest edge T_e gradients.

The question now is whether the shine-through of downshifted thermal radiation can quantitatively account for the enhanced emission observed on ASDEX Upgrade. In order to check this, the ECE spectrum is simulated assuming purely thermal electron velocity distribution at each location. $T_e(r)$ is taken from Thomson scattering measurements. The ECE intensity at each frequency is calculated taking into account the radiation transport by emission and re-absorption. The absorption coefficient is determined from experimental T_e and n_e profiles (the latter obtained from combined deconvolution of interferometer line averages and edge Li-beam measurements). Figure 8, the experimental T_e and n_e profiles are shown together with the interpolated T_e profile used for the calculations. The

temperature outside the separatrix is assumed zero. Figure 9 shows the simulated (line) and measured (asterisks) radiation temperature. The measured pronounced enhanced radiation maximum is *not* reproduced by the simulation. Although wall reflection, not accounted for in the simulations, might lead to somewhat larger radiation temperatures at the plasma edge, the difference between simulation and measurements is to large to be explained by this effect.

This result is not surprising in view of the discussion of section 1.5. For electron temperatures obtained on ASDEX Upgrade the frequency downshift and broadening translates into an apparent radial displacement from the resonant location of at most 8 mm at the plasma edge (from the point where $T_e = 1$ keV) or at most a few cm from the plasma centre (for T_e of several keV). This distance is too small to account for the radial extent of observed enhanced radiation up to 3 cm outside the separatrix even without considering re-absorption (assuming optical depth zero). In addition, at high optical depth (which is almost always found closely inside the separatrix for the discharges of interest because of the steep n_e and T_e gradients during H-mode), the down-shifted radiation will be mostly re-absorbed. Only the region near the separatrix remains, but there T_e is below 300 eV and therefore the down-shift results in a displacement of only 1 mm or less, which cannot account for the observed effect.

We conclude from the considerations above that the observation of enhanced ECE radiation temperature at the plasma edge is incompatible with a thermal electron velocity distribution. As a consequence, we subsequently focus on mechanisms which can lead to non-Maxwellian distribution functions at the plasma edge.

2.4 Effect of neutral beam heating on ECE

From the discussion in the previous section it is concluded that the emission maximum in the ECE spectrum outside the separatrix must have a nonthermal origin. If a non-thermal population is assumed to exist just inside the last closed flux surface, the observed down shift of the emission maximum of $1 - 2$ GHz corresponds to electron energies between 5 and 10 keV. The discharges described here are heated by neutral beam injection, hence we first discuss the possible effect of this heating method on the generation of fast electrons.

The energy of the injected deuterium neutrals in ASDEX Upgrade is about 60 keV. The maximum energy transferred to an electron by a 60 keV-ion (head-on collision) is $4E_i(m_e/m_i)$ or about 64 eV, so that single ion-electron collisions cannot produce an electron population at several keV energy. Nevertheless, an important part of the injected power is transferred to the electrons through slowing down of the high energy ions, this energy goes mainly to low energy electrons, which thermalize on a short timescale.

For the electrons responsible for the nonthermal radiation an estimate of the importance of the collisions with ions can be made by comparing the terms in the ion-electron collision operator with the terms in the electron-electron collision operator. Using the high velocity limit [13] it can be shown that the diffusion coefficients in momentum space satisfy

$$\frac{D_{pp}^{ie}}{D_{pp}^{ee}} = \frac{n_i q_i^2 m_e E_i}{n_e q_e^2 m_i T_e} \ll 1. \qquad (6)$$

Here D_{pp}^{ie} (D_{pp}^{ee}) is the diffusion coefficient in momentum space due to ion-electron (electron-electron) collisions, n_i (n_e) is the number density of the high energy ions (electrons), q_i,

m_i, and E_i (q_e, m_e, and T_e) are the ion (energy) charge, mass, and temperature. Due to the large mass difference between electrons and ions and the small number density of the high energy ions it follows that the diffusion due to ion-electron collision is always much smaller than the diffusion (equilibration) due to electron-electron collisions, and no nonthermal effects are generated.

2.5 Effect of loop voltage on ECE spectra

Confinement in a tokamak relies on a plasma current, which in ASDEX Upgrade, like in most other tokamaks, is almost entirely inductively driven. The necessary loop voltage accelerates electrons parallel to the magnetic field. However, the ECE method is sensitive to the electron velocity in the perpendicular direction only, so that a fast electron tail must undergo pitch angle scattering to be noticed in ECE measurements.

The energy (E_c) beyond which a flat tail on the distribution function is formed can be estimated from the Dreicer formula to be

$$E_c = 0.13\, n_{19} \ln\Lambda / E_{\|} \quad \text{(keV)}, \tag{7}$$

where n_{19} is the density in units of 10^{19} m^{-3}, $E_{\|}$ is the electric field component parallel to the magnetic field in V/m, and $\ln\Lambda$ is the Coulomb logarithm. For $n_e \approx 1 \times 10^{19}$ m^{-3}, $E_{\|} \approx 0.05$ V/m, and $\ln\Lambda \approx 15$, one finds that a flat tail is formed beyond the energy $E_c = 39$ keV. Electrons at higher energies are essentially collisionless and "run away", whereas those at lower energies equilibrate within the thermal distribution.

This energy is far larger than the estimated energy of the electrons that responsible for the emission of the nonthermal radiation. Therefore one does not expect the electric field to have a large influence on the ECE spectrum. Nevertheless, the distribution is also deformed for energies below the energy of equation 7, and a quantitative analysis is necessary to determine the exact amount of nonthermal radiation.

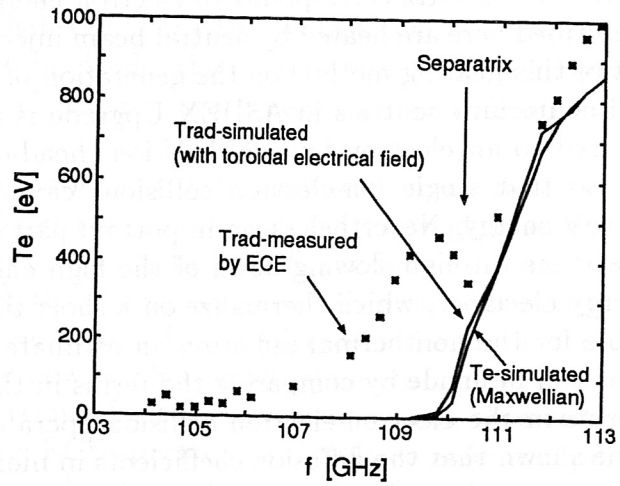

Figure 10: *Simulated T_{rad} spectrum (solid line) both for a Maxwellian distribution and including effect of downshifted radiation from electrons accelerated in the toroidal electrical field compared to the measured T_{rad} spectrum (symbols)*

This amount can be calculated from the distribution function obtained by the Fokker-Planck code described above. Figure 10 shows the obtained spectrum, together with the

Maxwellian spectrum, and the data points. It is clear from this figure that the acceleration by the parallel electric field leads only to a small increase of radiation compared with the Maxwellian case, and can not explain the observed phenomenon.

2.6 Effect of enhanced radial diffusion of fast electrons

As outlined in the previous sections, the observed anomalous radiation temperature peak in ECE spectra at the plasma edge cannot be quantitatively explained by effects of neutral beam injection or the toroidal electrical field on the electron distribution.

In this section, we investigate the possibility that enhanced anomalous radial transport create a fast electron population that leads to the observed radiation profile. As the number of electrons of energy E in the high energy tail of a thermal distribution increases strongly with temperature, $f(E) \propto \exp(-E/kT)$, a relatively large amount of fast electrons with $E \geq 5$ keV exists a few centimeters inside the separatrix during H-mode, which is characterised by extremely steep temperature and density profiles at the edge. In general, the downshifted radiation of these electrons is not visible from the low field side due to large optical thickness. If radial transport of these high energy electron is sufficiently fast, the above-thermal population at the separatrix can be enhanced. Down-shifted radiation from the separatrix can be observed when, in cases of low optical thickness in the scrape-off-layer (SOL) and further outside, re-absorption is weak.

This mechanism can explain the strong dependence of the nonthermal radiation on the temperature gradient. The amount of electrons with an energy around 5 keV depends exponentially on the electron temperature, and therefore a sufficient large temperature a few centimetres inside the separatrix, i.e. a sufficient large temperature gradient, is expected to be a necessary condition for a nonthermal contribution in the ECE spectrum. Also, quenching of the enhanced radiation at high density can possibly be interpreted as being due to a shorter slowing down time as explained below. It might, however, also be that a high electron density at the edge is correlated with a low temperature gradient.

We now estimate the transport enhancement necessary for a significant distortion of the distribution function. Assuming diffusive transport, which is described in terms of a diffusion coefficient D (which may depend on particle energy), the typical timescale τ_d for transport over a distance Δr is

$$\tau_d = \Delta r^2 / D.$$

Transport will distort the distribution function from Maxwellian if the transport time scale τ_d is short compared to the relaxation time (slowing down time) τ_s of the fast electrons to the local thermal distribution. For high electron energy E_k, this can be approximated as:

$$\tau_s = 2 \cdot 10^{-5} E_k^{3/2} / n_{19} \text{ s},$$

where E_k is the energy measured in keV. When the slowing down time is shorter than the transport timescale the electrons loose their energy before they can be transported into the optical thin layer and no contribution to the nonthermal spectrum occurs. This condition yields a minimum value for the diffusion coefficient

$$D > 5 \cdot 10^4 \Delta r^2 E_k^{-3/2} n_{19}.$$

For a radial distance $\Delta r = 2$ cm, $E_k = 5$ keV and $n_{19} = 1$ the minimum particle diffusion coefficient is $D > 1.8$ m^2/s. This value is significant larger than the typical values for

thermal electrons in the edge gradient region during H-mode: $D \approx 0.2$ m^2/s (averaged) during type-I ELMy H-mode, and $D \approx 0.05$ m^2/s in phases between two type-I ELMs [14]. However, high energy electrons do not necessarily have the same transport properties as the thermal electrons.

We now determine the enhanced transport (as described by the value of D) necessary to explain the observed ECE spectra. Again, this is done by using the combination of the *RELAX* 3D Fokker-Planck transport and *NOTEC* ECE simulation codes.

The diffusion coefficient D must be assumed energy dependent as to preserve the good confinement of thermal electrons. We choose the ansatz

$$D = \alpha E_k^{1/2}. \tag{8}$$

The electron density is kept constant and equal to the measured density profile by introduction of an inward pinch V, which is independent of energy

$$V = -\frac{\frac{\partial}{\partial r}\int \mathrm{d}^3 p D(p) f(p,\theta,r)}{\int \mathrm{d}^3 p f(p,\theta,r)}.$$

Here, $f(p,\theta,r)$ is the velocity distribution which is a function of momentum p, pitch angle θ and the radial coordinate r. Because the outward flux of high energy electrons is mostly compensated for by an inward pinch of bulk electrons, the introduced pinch does not significantly influence the nonthermal part of the distribution function.

The radial electric field in the plasma edge is not accounted for in the simulations. Although this field can be as large as 10 keV/m the electrons are transported over a few cm only and their change in energy is a few hundred eV. This change in energy is small compared to the temperature at the location where the electrons are generated. Although the electric field might have an influence, it is expected that the difference in radiation temperature at the plasma edge is smaller than 30 %.

The boundary condition in the scrape-off layer is formulated as follows. It is assumed that the electrons outside the separatrix that can overcome the magnetic mirror formed by the toroidal magnetic field move along the field lines into the divertor and are lost on the timescale τ_{ls}

$$\tau_{ls} = \frac{1}{2}\int \frac{\mathrm{d}s}{v_\parallel(s)},$$

where the integration is along the field line. Because the mobility of the electrons is much larger than that of the ions it is assumed that a small parallel electric field exists that confines the low energy electrons. The influence of this field is modelled by a particle source with a Maxwellian distribution with a temperature of $T_r = 20$ eV. The boundary condition can, therefore, be written as

$$\frac{\partial f}{\partial t} = -\frac{f_{\text{not trapped}}}{\tau_{ls}} + A\exp\left(-\frac{E}{T_r}\right),$$

where the coefficient A is given by the condition of constant density

$$A = \frac{1}{\tau_{ls}}\frac{\int \mathrm{d}^3 p f_{\text{not trapped}}}{\int \mathrm{d}^3 p \exp[-E/T_r]}.$$

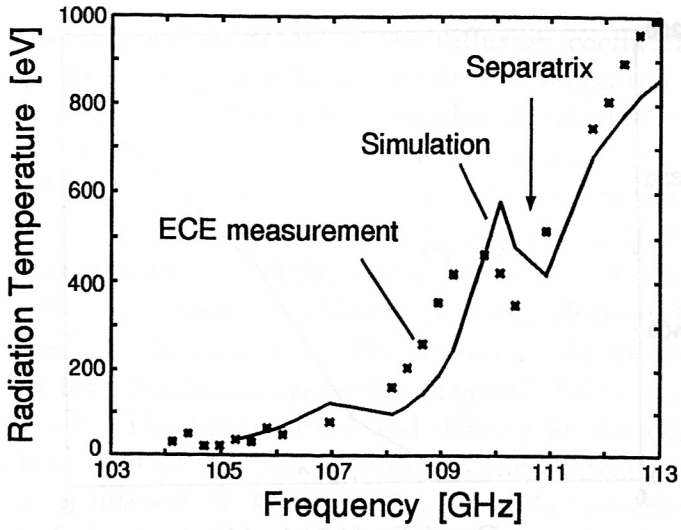

Figure 11: *Simulated T_{rad} spectrum (solid line) assuming enhanced fast particle diffusion ($D = 2\ m^2/s\ E_k^{1/2}$, E_k in keV) compared to T_{rad} spectrum measured by ECE.*

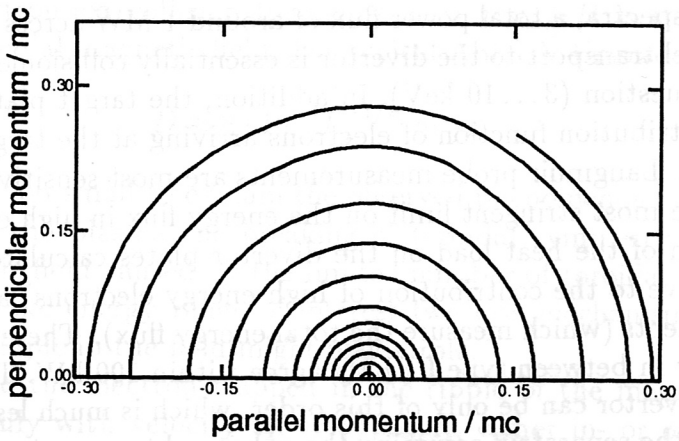

Figure 12: *Steady-state distribution function just inside the separatrix ($\rho_{pol} = 0.996$) leading to enhanced ECE emission.*

In Fig. 11 the *NOTEC* results of a simulation with $\alpha = 2$ are shown together with the measurements for comparison. This simulations shows that the proposed mechanism is indeed possible. Figure 12 is a contour plot of the steady state distribution function for $\rho_{pol} = 0.996$ (just inside the separatrix). This distribution function show a bulk distribution with a low temperature. For higher energies, however, an asymmetric nonthermal distribution is generated due to the radial flux of high energetic electrons. Also the scaling of the radiation temperature outside the separatrix with the gradient of the temperature is reproduced by the simulations. Figure 13 shows the radiation temperature at the frequency $f = 110$ GHz for a constant diffusion coefficient as a function of the gradient in the electron temperature. The obtained scaling is similar to the experimental obtained scaling shown in figure 6.

An important consequence of a radial transport enhancement of fast electron is that a fraction of the power flux across the separatrix must be carried by fast particles. With the diffusion coefficient $D = \alpha E_k^{1/2}$ described above, which reproduces the observed cy-

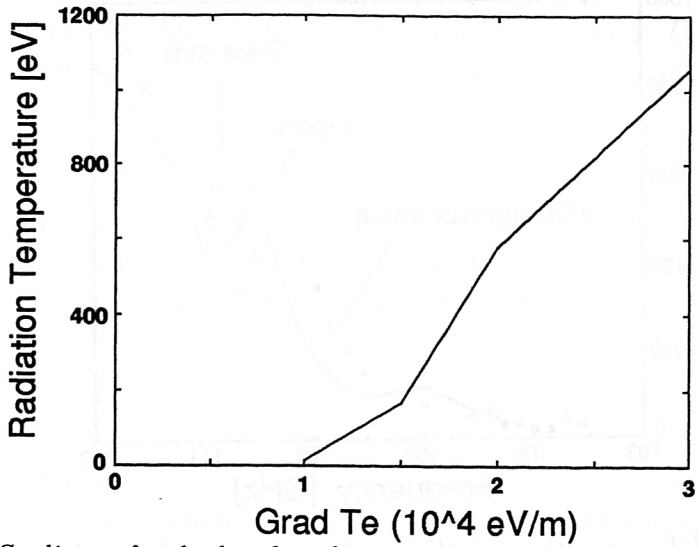

Figure 13: *Scaling of calculated radiation temperature at 110 GHz with the electron temperature gradient at the separatrix.*

clotron radiation spectra, a total power flux of around 1 MW across the separatrix can be estimated. Parallel transport to the divertor is essentially collisionless for electrons in the energy range in question (3...10 keV). In addition, the target plate sheath is transparent, hence the distribution function of electrons arriving at the target plate should show a high energy tail. Langmuir probe measurements are most sensitive to electron energies of several kT. The most stringent limit on the energy flux in high energy electrons is set by the comparison of the heat load on the divertor plates calculated from these probes (which is insensitive to the contribution of high energy electrons) and from the thermographic measurements (which measure the total energy flux). These measurements of the power flux density in between type I ELMs agree within 100 kW. The power flux of fast electrons to the divertor can be only of this order, which is much less than the estimated power flux across the separatrix assuming the enhanced transport coefficient Eq. 8 (with $\alpha = 2\ \mathrm{m}^2/\mathrm{s}$).

It follows that an *ad-hoc* ansatz like Eq. 8, though describing the observed ECE spectra reasonably well, predicts a high loss power of fast electrons not observed in the experiment. We note here that choice of the functional dependence of D on the energy is somewhat arbitrary, and that in the simulations no wall reflection was taken into account. Setting the diffusion coefficient to zero for energies below 7 keV, still gives reasonable agreement with the experiments, and leads to a total power flux over the separatrix of 350 kW. When wall reflection is taken into account, the fast electron population necessary to generate the observed spectra is smaller and carries a heat flux of below 100 kW. We, therefore, conclude that the explanation of the enhanced radiation is, with the present knowledge, not in contradiction with these measurements. Detailed analysis for different shots is necessary to set accurate errorbars on the measurements of the power flux in fast electrons.

2.7 Discussion of neo-classical transport

As shown in the previous paragraph a sufficient large radial transport can explain the observed nonthermal radiation, but no picture of a physical cause was given. It was

also seen that an arbitrary enhancement of the diffusion coefficient, not motivated by physics, may imply very large power fluxes across the separatrix associated with fast particles. In this section, we want to examine collision dominated transport as a physical mechanism for enhanced fast particle loss. Several estimates will be made of the relevant particle diffusion coefficients for typical edge parameters in ASDEX Upgrade. The same parameter set is used throughout: density $n_{19} = 1$, magnetic field $B = 2$ T, Major radius $R = 2$ m, inverse aspect ratio $\epsilon = 0.25$, safety factor $q = 3$, strength of the rippled magnetic field $\delta = 0.01$, and number of field coils $N = 16$, effective charge $Z_{\text{eff}} \approx 1$. It will be shown that neo-classical transport is insufficient to explain the observed phenomenon.

First the transport for a toroidally symmetric magnetic field configuration (no toroidal field ripple) is discussed. The temperature and density at the edge are such that the relevant regime for transport of the bulk electrons is the Plateau or the Pfirsch-Schlüter regime. The electrons of interest, however, have much higher energies and their transport coefficients are that of the banana regime. Using the usual estimate [15], the particle diffusion coefficient is

$$D \approx \sqrt{\epsilon}\nu_{ei}\rho^2\left(\frac{B}{B_\theta}\right)^2,$$

where ν_{ei} is the electron-ion collision frequency, $\rho = mv_\perp/eB$ is the gyroradius, and $B_\theta \approx \epsilon B/q$ is the poloidal magnetic field. For typical ASDEX Upgrade parameters

$$D \approx 8 \cdot 10^{-3} E_k^{-1/2} \text{ m}^2/\text{s}.$$

This coefficient is far too small to explain the observed phenomenon.

Near the edge of the plasma the breaking of toroidal symmetry also plays a role. The 'rippled' magnetic field caused by the limited number of toroidal field coils leads to additional losses. In the energy range of interest two loss mechanisms which are both connected with this ripple in the field might play a role.

The first is due to the electron trapped in the ripple of the magnetic field. These electrons drift vertically with velocity $v_D = v_\perp^2/2\omega_c R$, either in- or outward until they are detrapped by Coulomb collisions. The detrapping time is proportional to the ripple strength $\delta = \Delta B/B$, which for ASDEX Upgrade is around 1 % at the edge. Because the fraction of particles trapped by the ripple is roughly $\sqrt{\delta}$, the diffusion coefficient can be estimated to be [16]

$$D = \frac{1}{2}\delta^{3/2} v_d^2 \tau_c,$$

where τ_c is the collision time for 90° angle scattering. For typical ASDEX Upgrade parameters one finds

$$D \approx 1 \cdot 10^{-3} E_k^{7/2}. \tag{9}$$

The losses due to this mechanism are insufficient to explain the observed phenomenon. It must be pointed out too, that the estimate given above is not valid for the entire energy range. At higher energies the diffusion coefficient is large and the electrons trapped in the ripple are lost from the plasma rapidly. The distribution function forms a loss cone when the timescale for scattering into the ripple trapped particle region of velocity space, which is the collision time of 90° angle scattering, is longer than the transport timescale.

The second mechanism is connected with electrons which can freely overcome the ripple in the magnetic field but are trapped in the magnetic mirror formed by the change

of the toroidal magnetic field over the flux surface. The transport for the energy range of interest is determined by the ripple plateau regime [17]. In the more collisional case the electrons with low pitch suffer significant collisions while crossing a single phase of the ripple. The drift due to the ripple then causes a random walk of the electrons. In the less collisional case the electrons, while moving along the field line, average the ripple except near its turning points. When collisional scattering is sufficiently strong the electrons bounce at random ripple phase. A random walk in radial direction then occurs because an electron drifts over a different radial distance every time it bounces. The diffusion coefficient for the more collisional case and the less collisional case are equal and given by

$$D = \frac{1}{4\sqrt{2}} N \langle \delta^2 \rangle \rho^2 \left(\frac{B}{B_\theta} \right)^2 \frac{v}{R}, \tag{10}$$

which, for typical parameters in ASDEX Upgrade, is

$$D = 1 \cdot 10^{-3} E_k^{3/2} \ \mathrm{m}^2/\mathrm{s}.$$

Again this diffusion coefficient is insufficient to explain the observed phenomenon.

Also this estimate is not valid over the entire energy range. As already mentioned the collisional scattering must be sufficient strong to scatter an electron within a bounce time over a pitch angle large enough for the electron to bounce at random ripple phase. This is the case when

$$\tau_c < \frac{q^3 N^2 R}{\epsilon^{3/2} v},$$

which for ASDEX Upgrade is

$$E_k < 60.$$

In conclusion, the collision dominated transport is insufficient to explain the observed phenomenon.

The implication for ions

Although not of direct interest for the ECE, it is interesting to study the implication for the ions. Also for the ions radial transport might lead to a nonthermal velocity distribution at the edge of the plasma. Because the slowing down time is a factor $\sqrt{m_i/m_e}$ larger, smaller diffusion coefficients are sufficient to generate the effect. Furthermore, all collision dominated diffusion coefficients discussed above are a factor $\sqrt{m_i/m_e}$ larger and, therefore, are no longer insignificant. Setting the transport timescale equal to the slowing down time and using Eq. 9, the radial distance over which a Deuterium ion can be transported can be calculated

$$\Delta r_D \approx E_k^{7/2} n_1 9^{-1/2} \ \mathrm{cm}.$$

For energies of a few keV this distance can be rather large. It must, however, be noted that the magnitude of the ripple decreases toward the plasma centre, and the estimate is no longer valid for large distances.

3 Summary and conclusions

Diagnostics of the radial electron temperature profile in a tokamak by radiometry of the electron cyclotron emission is limited by a number of effects. Using high harmonics of the cyclotron frequency is desirable to have access to the resonant region at high densities. However, low optical thickness and harmonic overlap impose a severe limit on the harmonic number. In almost all cases, the second harmonic in X-mode is preferable for ECE measurements of T_e. We find that for ASDEX Upgrade, optical thickness even at the plasma boundary is sufficient for all but the lowest values of the $n_e \times T_e$-product. High-n_e cutoff is a practical problem for low magnetic fields B_t, especially for high densities such as frequently obtained in H-mode.

A new phenomenon arises when very steep edge T_e gradients and low densities are encountered, as often obtained during type-I ELMy H-modes. In these cases, enhanced emission can occur, i.e. the radiation temperature assumes a value quite above the true electron temperature. This effect often manifests itself as a pronounced radiation maximum at frequencies resonant at or slightly outside the plasma boundary. From analytic estimates of the relativistic and Doppler shifts as well as from numerical simulations of ECE spectra we conclude that a Maxwellian electron distribution described at each radius cannot explain the observations quantitatively. We conclude that a non-thermal distribution must exist at high ∇T_e and low n_e. Since the ECE method is particularly sensitive to the high energy tail of the electron distribution, only a small amount of fast electron is necessary to explain the observed phenomenon. However, we find from numerical Fokker-Planck calculations that neither neutral beam heating nor the toroidal electrical field (loop voltage) can distort the electron distribution sufficiently to reproduce the observed spectra.

A high energy tail can be generated if enhanced transport of fast electrons from regions at higher temperature is assumed. We find that simulations with a diffusion coefficient around 3 m^2/s for $E = 5$ keV indeed can reproduce the enhanced radiation feature in the measurement. The question, however, is how fast particle diffusion can be enhanced, in particular during phases of improved confinement of the thermal distribution. Additional losses due to particles trapped in the toroidal field ripple as well as the plateau regime transport are still about one order of magnitude too small to account for the required transport enhancement. At this stage of diagnostics, no conclusive statement on the origin of the observed anomaly seems possible. We may speculate, that, since the phenomenon occurs under conditions of high pressure gradient at the plasma edge, there may be a relation to instability-driven anomalous transport. However, more experimental and theoretical evidence of fast particle transport in general is necessary to establish such a connection to the distribution function perturbation discussed above.

References

[1] M. Bornatici, R. Cano, O. de Barbieri, F. Engelmann, Nuclear Fusion, **23** 1153 (1983)

[2] Z. Wang *et. al.*, General Atomics Report GA-A22038 (1995)

[3] D. V. Bartlett *et. al.*, Proceedings of the 19th EPS Innsbruck (1992) 1-49, p. I-163 ff.

[4] A. Airoldi and G. Ramponi, Proceedings of the 20th EPS Lisbon (1993) 6-39, p. III-1223 ff.

[5] C. P. Tanzi, Ph.D. thesis, Technische Universiteit Eindhoven and FOM-Instituut voor plasmaphysica "Rijnhuizen" 1996

[6] D. V. Bartlett, *Physics Issues of ECE and ECA for ITER*, JET Report JET-P(95)46 (1995)

[7] G. Cima, *Thermal, nonthermal and stimulated fluctuations of tokamak electron cyclotron radiation* Fusion Research Center Report FRCR #390 (1991), The University of Texas at Austin, DOE/ER/53267-86

[8] S. Sattler, H. J. Hartfuß, Plasma Phys. Control. Fusion **35**, 1285 (1993), S. Sattler, H. J. Hartfuß, and W VII-AS Team, Phys. Rev. Lett. **72**, 653 (1994)

[9] M. Häse, H. J. Hartfuß, Verhandl. DPG (VI) **31**, 735, P10.6 (1996)

[10] A. Janos *et. al.*, Plasma Phys. Contr. Fusion **38**, 1373 (1996)

[11] E. Westerhof, A. G. Peeters, W. Schippers, *RELAX, a computer code for the study of collisional and wave-driven relaxation of the electron distribution function in toroidal geometry*, Rijnhuizen Report **92-211** (1992). National Technical Information Service Document No. DE95703278.

[12] R. M. J. Sillen, M. A. F. Allaart, W. J. Goedheer, and A. Kattenberg, *NOTEC, a computer code to simulate ECE spectra of plasmas which include nonthermal populations*, Rijnhuizen Report **86-165** (1986). This code was adapted by E. Westerhof to calculate ECE spectra for arbitrary distribution functions and by A. G. Peeters to include the specific ASDEX Upgrade equilibrium.

[13] C. F. F. Karney, Comp. Phys. Reports **4**, 183 (1986)

[14] H. Reimerdes, Diploma thesis, IPP Garching and Universität Bayreuth (1996) IPP Report 1/300

[15] A. A. Galeev, Neo-classical theory of transport processes, in: Advances in Plasma Physics **3**, John Wiley & Sons, New York (1974)

[16] R.B. White, Theory of tokamak plasmas, North Holland, Amsterdam, (1989)

[17] A. Boozer, Phys. Fluids **23**, 2283 (1980)